Cell Reports, Volume *27*

Supplemental Information

Mutant FUS and ELAVL4 (HuD) Aberrant Crosstalk in Amyotrophic Lateral Sclerosis

Riccardo De Santis, Vincenzo Alfano, Valeria de Turris, Alessio Colantoni, Laura Santini, Maria Giovanna Garone, Giuseppe Antonacci, Giovanna Peruzzi, Emma Sudria-Lopez, Emanuel Wyler, Jasper J. Anink, Eleonora Aronica, Markus Landthaler, R. Jeroen Pasterkamp, Irene Bozzoni, and Alessandro Rosa

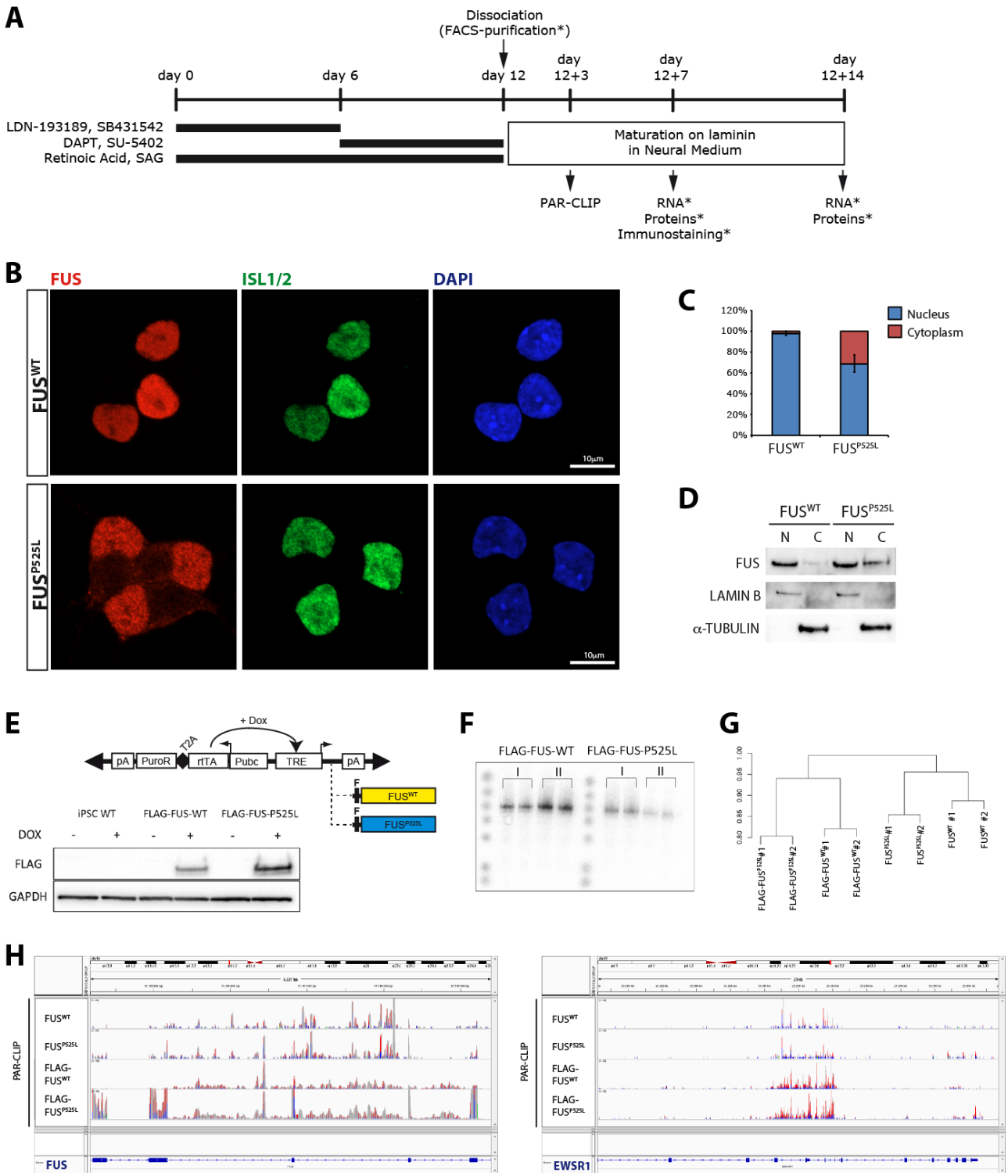

Figure S1. Human iPSC motor neuron differentiation and FUS PAR-CLIP, Related to Figure 1

(A) Schematic representation of the human iPSC motor neuron differentiation protocol and time points of the analyses described in the main text. The asterisk marks analyses that have been performed on FACS-purified motor neurons. (B) Single channels of the

immunostaining reported in Figure 1A, showing FUS localization (red) in FACS-purified MNs (day 12+7). ISL1/2 (green) marks MNs and DAPI (blue) the nuclei. Scale bar: 10 μm. (C) Quantification of the fraction of nuclear and cytoplasmic FUS in FUS^{WT} and FUS^{P525L} FACS-purified motor neurons (day 12+7) from immunofluorescence images. (D) Cytoplasmic fractionation was performed in iPSC-derived MNs (day 12+3 of differentiation) using a hypotonic lysis buffer (HEPES-KOH 10 mM, EDTA 0.1 mM, 0.5% (v/v) NP40, KCl 10 mM, DTT 1 mM and complete EDTA-free protease inhibitor cocktail) for 10 minutes on ice. Supernatant was considered cytoplasmic extract, while pellet nuclei. The pellets were washed using hypotonic buffer to completely clean the samples from the cytoplasmic extract. Cell pellets were then resuspended in hypertonic lysis buffer (50 mM HEPES-KOH, 150 mM KCl, 2 mM EDTA, 1 mM NaF, 0.5% (v/v) NP40, 0.5 mM DTT and complete EDTA-free protease inhibitor cocktail) and incubated for 15 minutes on ice. Western blot analysis was performed as described in the main text using anti-ELAVL4 (1:1000, sc-48421; Santa Cruz Biotechnology), anti-FUS (1:800, sc-47711; Santa Cruz Biotechnology), anti-LAMIN B (1:250, sc-6216; Santa Cruz Biotechnology), anti-α-TUBULIN (1:10000, T6199, Sigma-Aldrich) primary antibodies. (E) Upper panel, schematic representation of the enhanced piggyBac transposable vector for doxycycline conditional expression of FLAG-FUS^{WT} (epB-Puro-TT-FLAG-FUS^{WT}) and FLAG-FUS^{P525L} (epB-Puro-TT-FLAG-FUS^{P525L}). F: FLAG tag; pA: polyadenylation signal; PuroR: puromycin resistance gene; T2A: self-cleavage peptide; rtTA: TET transactivator protein gene; Pubc: human Ubiquitin C constitutive promoter; TRE: TET responsive element; Dox: doxycycline. Triangles represent terminal repeats of the transposon. Lower panel, doxycycline-dependent expression of FLAG-FUS^{WT} and FLAG-FUS^{P525L} in iPSCs, reveled by western blot using an anti-FLAG antibody. GAPDH has been used as a loading control. (F) Representative autoradiograph image of FUS-RNA complexes radiolabeled at RNA 5' end and purified in PAR-CLIP experiments, 2 lanes for each replicate, biological replicates = 2, for FLAG-FUS^{WT} and FLAG-FUS^{P525L} ectopically expressed in MNs. (G) Cluster dendrogram showing the correlation matrix between samples used for the PAR-CLIP. (H) Snapshot of the IGV window showing the mapping of PAR-CLIP reads and transitions on two known interactors of FUS^{WT}, EWSR1 and FUS intron 7-8.

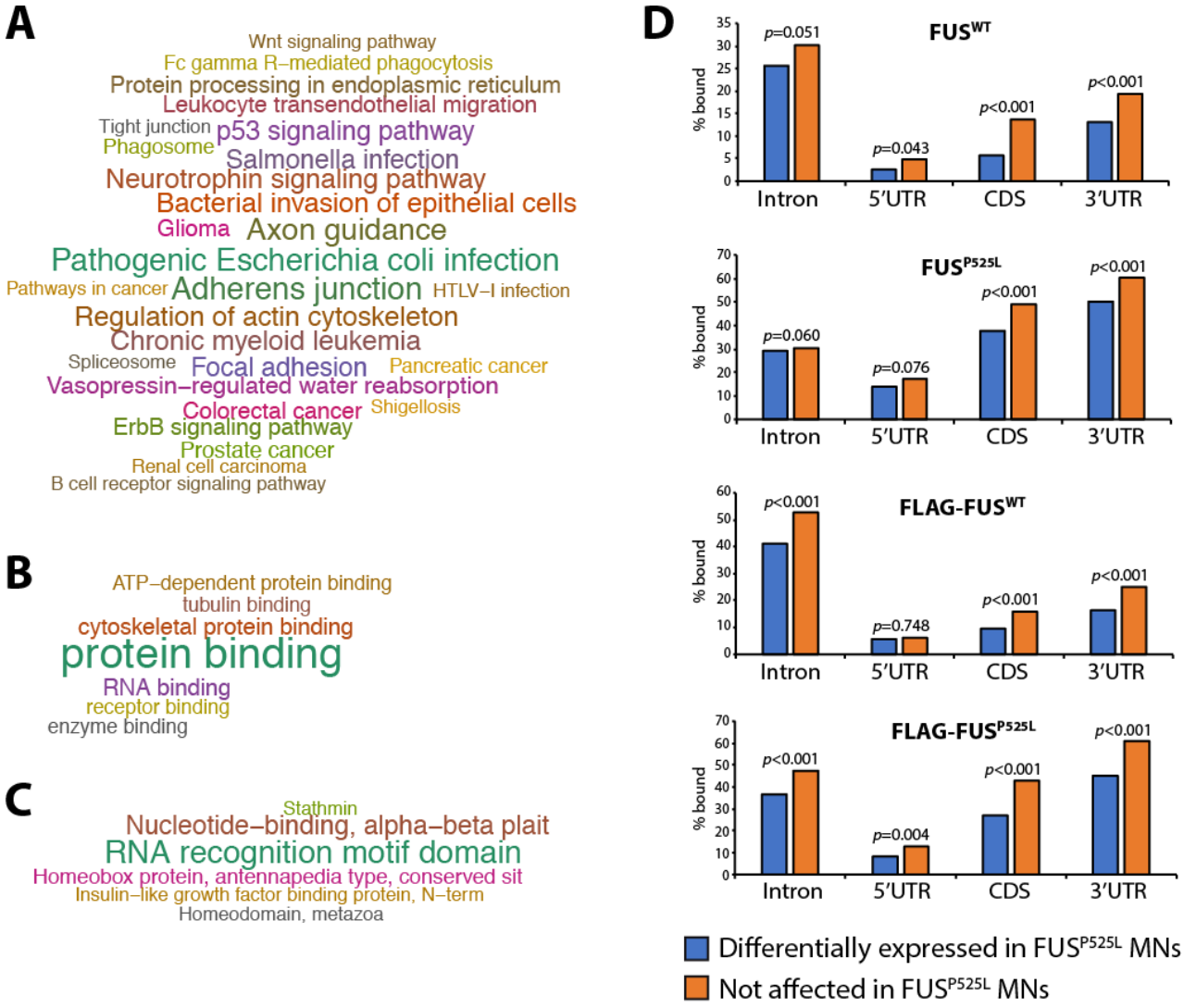
A
Wnt signaling pathway
Fc gamma R–mediated phagocytosis
Protein processing in endoplasmic reticulum
Leukocyte transendothelial migration
Tight junction
p53 signaling pathway
Phagosome
Salmonella infection
Neurotrophin signaling pathway
Bacterial invasion of epithelial cells
Glioma
Axon guidance
Pathogenic Escherichia coli infection
Pathways in cancer
Adherens junction
HTLV–I infection
Regulation of actin cytoskeleton
Chronic myeloid leukemia
Spliceosome
Focal adhesion
Pancreatic cancer
Vasopressin–regulated water reabsorption
Colorectal cancer
Shigellosis
ErbB signaling pathway
Prostate cancer
Renal cell carcinoma
B cell receptor signaling pathway
B
ATP–dependent protein binding
tubulin binding
cytoskeletal protein binding
protein binding
RNA binding
receptor binding
enzyme binding
C
Stathmin
Nucleotide–binding, alpha–beta plait
RNA recognition motif domain
Homeobox protein, antennapedia type, conserved sit
Insulin–like growth factor binding protein, N–term
Homeodomain, metazoa
D
FUSWT
FUSP525L
FLAG-FUSWT
FLAG-FUSP525L
% bound
p=0.051
p=0.043
p<0.001
p=0.060
p=0.076
p=0.748
p=0.004
Intron
5'UTR
CDS
3'UTR
Differentially expressed in FUSP525L MNs
Not affected in FUSP525L MNs
E
FUSWT PAR-CLIP in MNs
(present work)
FUSP525L PAR-CLIP in MNs
(present work)
15
226
0
64
4197
130
36
2118
3608
23
1108
90
951
11
343
Brain cortex CLIP-seq
(Lagier-Tourenne et al., 2012)
Human MN transcriptome
(De Santis et al., 2017)

Figure S2. Analysis of FUS PAR-CLIP data, Related to Figure 1

(A) GO word-cloud representation of terms enriched in FUS^{P525L} 3'UTR-bound targets, showing KEGG pathways using the FIDEA tool (D'Andrea et al., 2013). (B-C) Word cloud generated by FIDEA representing GO Molecular Functions (B) and InterPro (C) terms enriched in the set of FUS^{P525L} 3'UTR-bound targets with more than 10% of T-C transitions in the 3'UTR. The categories are represented with a character size proportional to the statistical significance of their enrichment. (D) Fraction of FUS-bound mRNAs, with at least one T-C transition in the PAR-CLIP analysis, that are differentially expressed (blue bars; $p<0.05$) or not affected (orange bars; $p>0.05$) in FUS^{P525L} MNs previously analyzed by RNA-seq (De Santis et al., 2017). (E) Venn diagram showing the overlap between genes identified as targets of FUS^{WT} and FUS^{P525L} in human motor neurons (present work), as targets of FUS in human brain cortex from control individuals (Lagier-Tourenne et al., 2012), and as transcripts expressed in pure populations of human iPSC-derived motor neurons (De Santis et al., 2017). Peaks of binding in human brain cortex were identified by re-analysis of original data from Lagier-Tourenne et al. (2012), as described in De Santis et al. (2017).

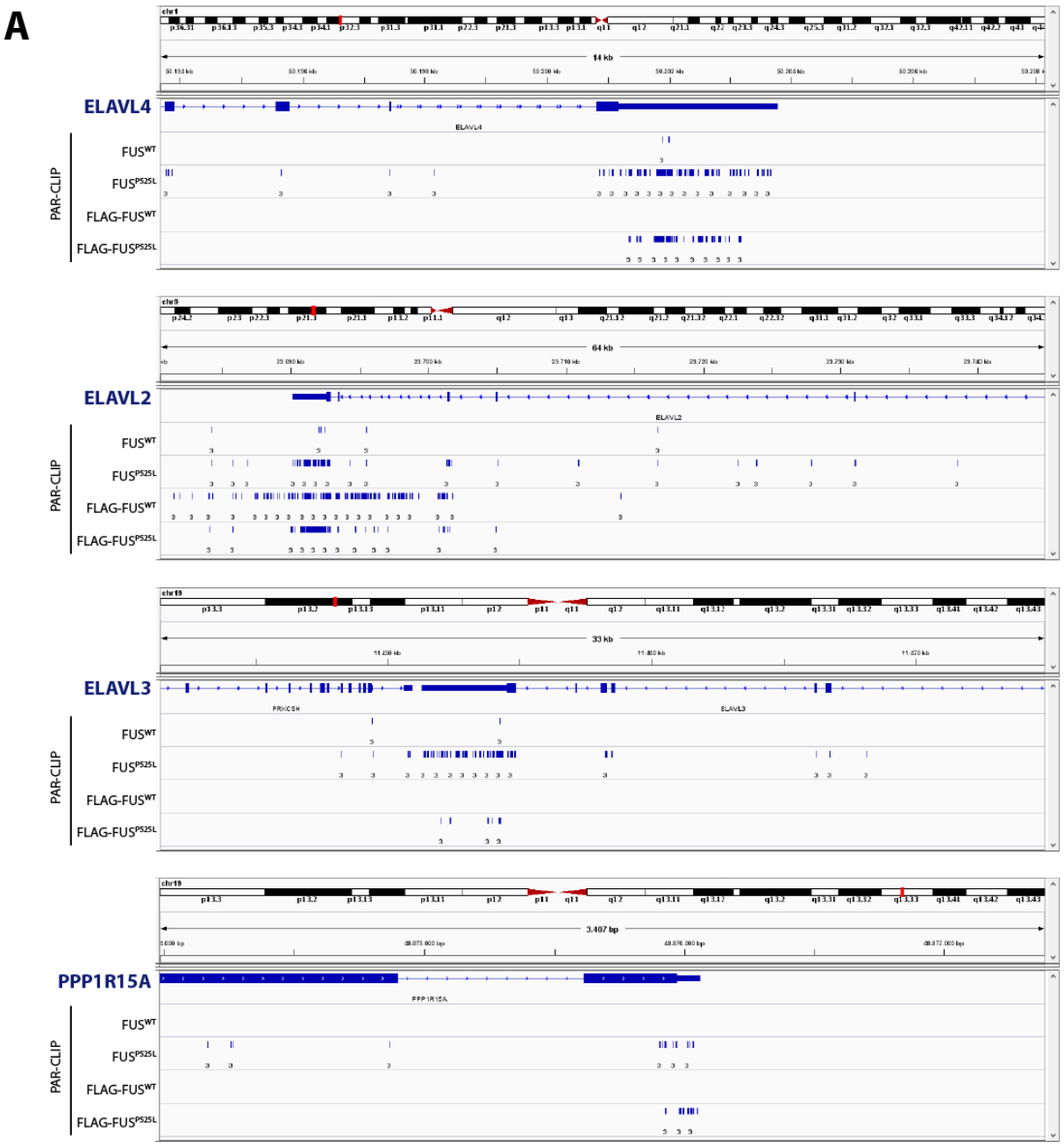
A
ELAVL4
ELAVL2
ELAVL3
PPP1R15A
PAR-CLIP
FUS^WT
FUS^P525L
FLAG-FUS^WT
FLAG-FUS^P525L

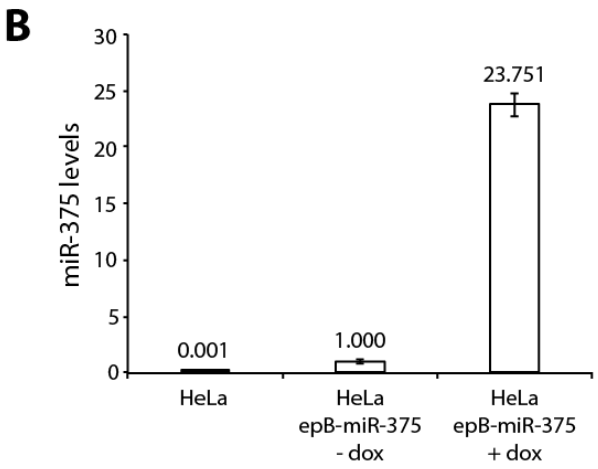
B
miR-375 levels
30
25
20
15
10
5
0
0.001
1.000
23.751
HeLa
HeLa epB-miR-375 - dox
HeLa epB-miR-375 + dox

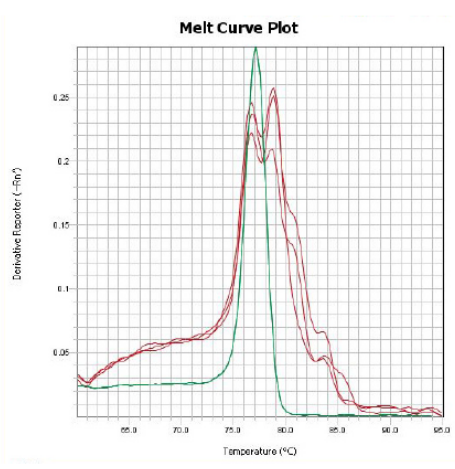
C
Melt Curve Plot
Derivative Reporter (-Rn')
Temperature (°C)

Figure S3. FUS 3'UTR targets and analysis of miR-375 expression in HeLa, Related to Figure 2

(A) Snapshot of the IGV window showing the mapping of PAR-CLIP T-C transitions on ELAVL4, ELAVL2, ELAVL3 and PPP1R15A 3'UTRs in FUS^{WT}, FUS^{P525L}, FLAG-FUS^{WT} and FLAG-FUS^{P525L} PAR-CLIP data sets. (B) Real time qRT-PCR quantification of the expression of miR-375, carried out as previously described (De Santis et al., 2017). HeLa cells that ectopically express miR-375 using a doxycycline inducible piggyBac transposon (epB-miR-375) have been used as positive control. Histogram bars represent the average of a technical triplicate, relative to the HeLa epB-miR-375 - dox sample that was set as 1, and error bars indicate the standard deviation. miR-375 was undetectable in untransfected cells (HeLa). (C) Melting curves of real time qRT-PCR products. The green line refers to the positive control (HeLa epB-miR-375 + dox), while red lines refer to untransfected cells.

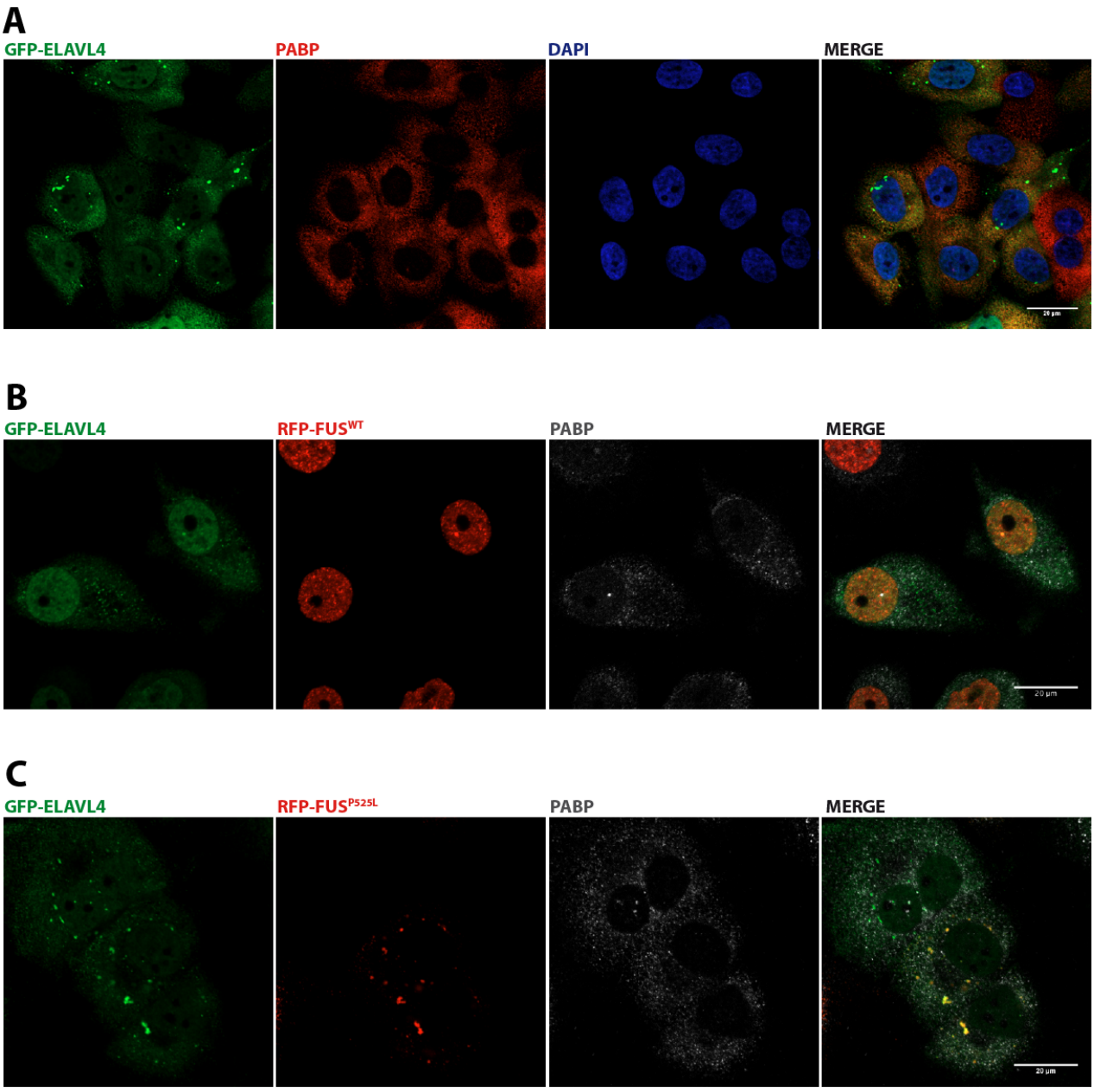
A
GFP-ELAVL4
PABP
DAPI
MERGE
B
GFP-ELAVL4
RFP-FUS^WT
PABP
MERGE
C
GFP-ELAVL4
RFP-FUS^P525L
PABP
MERGE
D
RFP-FUS^P525L
7.4
8
Brillouin shift (GHz)
10µm
E
GFP-ELAVL4
7.4
8
Brillouin shift (GHz)
10µm
F
Input
IP: ELAVL4
IgG
FUS^P525L
ELAVL4

Figure S4. Analysis of cytoplasmic speckles containing GFP-ELAVL4 and RFP-FUS^{P525L}, Related to Figure 3

(A) HeLa cells were stably transduced with the epB-Bsd-TT-GFP-ELAVL4 vector and induced with doxycycline for 24h. Confocal images show the GFP signal and immunostaining for the SGs marker PABP (red). DAPI (blue) marks nuclei. Scale bar: 20 μm. (B-C) Confocal images of HeLa cells stably transduced with the epB-Bsd-TT-GFP-ELAVL4 vector and the epB-Puro-TT-RFP-FUS^{WT} (B) or epB-Puro-TT-RFP-FUS^{P525L} (C) vector and induced with doxycycline for 24h. Confocal images show the GFP and RFP signals and immunostaining for the SGs marker PABP (white). DAPI (blue) marks nuclei. Scale bar: 20 μm. (D-E) Representative images acquired with the confocal microscope and with the BDB microscope of HeLa cells expressing RFP-FUS^{P525L} (panel E) or GFP-ELAVL4 (panel F). Scale bar: 10 μm. (F) Co-immunoprecipitation of RFP-FUS^{P525L} and GFP-ELAVL4 from cytoplasmic extracts of HeLa cells. Immunoprecipitation was performed using an anti-ELAVL4 antibody. In the western blot, RFP-FUS^{P525L} and GFP-ELAVL4 bands were revealed with an anti-FLAG antibody.

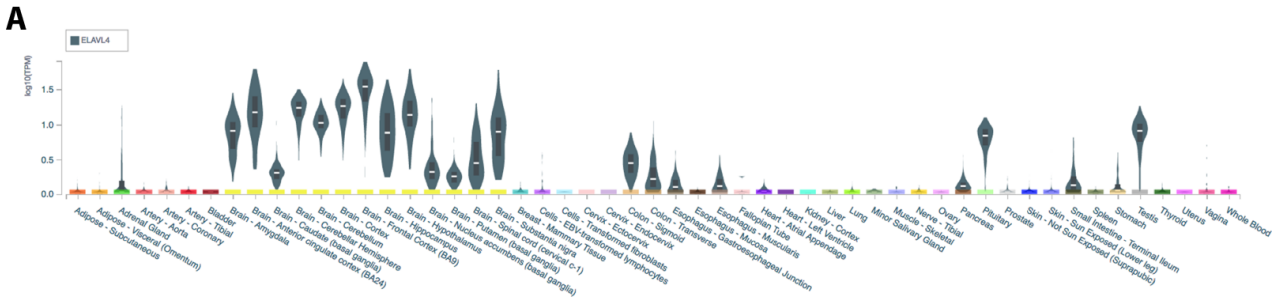
A
ELAVL4
log10(TPM)
1.5
1.0
0.5
0.0
Adipose - Subcutaneous
Adipose - Visceral (Omentum)
Adrenal Gland
Artery - Aorta
Artery - Coronary
Artery - Tibial
Bladder
Brain - Amygdala
Brain - Anterior cingulate cortex (BA24)
Brain - Caudate (basal ganglia)
Brain - Cerebellar Hemisphere
Brain - Cerebellum
Brain - Cortex
Brain - Frontal Cortex (BA9)
Brain - Hippocampus
Brain - Hypothalamus
Brain - Nucleus accumbens (basal ganglia)
Brain - Putamen (basal ganglia)
Brain - Spinal cord (cervical c-1)
Brain - Substantia nigra
Breast - Mammary Tissue
Cells - EBV-transformed lymphocytes
Cells - Transformed fibroblasts
Cervix - Ectocervix
Cervix - Endocervix
Colon - Sigmoid
Colon - Transverse
Esophagus - Gastroesophageal Junction
Esophagus - Mucosa
Esophagus - Muscularis
Fallopian Tube
Heart - Atrial Appendage
Heart - Left Ventricle
Kidney - Cortex
Liver
Lung
Minor Salivary Gland
Muscle - Skeletal
Nerve - Tibial
Ovary
Pancreas
Pituitary
Prostate
Skin - Not Sun Exposed (Suprapubic)
Skin - Sun Exposed (Lower leg)
Small Intestine - Terminal Ileum
Spleen
Stomach
Testis
Thyroid
Uterus
Vagina
Whole Blood

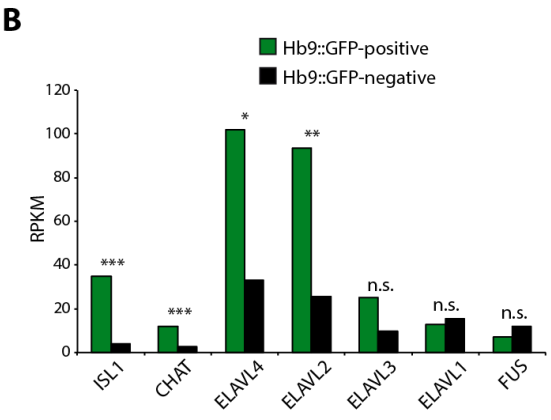
B
Hb9::GFP-positive
Hb9::GFP-negative
RPKM
120
100
80
60
40
20
0
***
***
*
**
n.s.
n.s.
n.s.
ISL1
CHAT
ELAVL4
ELAVL2
ELAVL3
ELAVL1
FUS

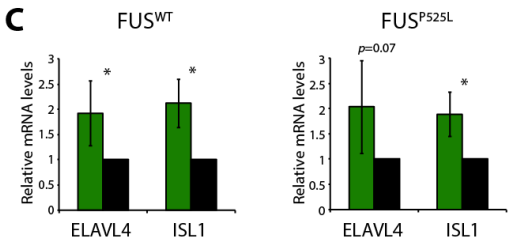
C
FUSWT
FUSP525L
Relative mRNA levels
3
2.5
2
1.5
1
0.5
0
*
*
p=0.07
*
ELAVL4
ISL1
ELAVL4
ISL1

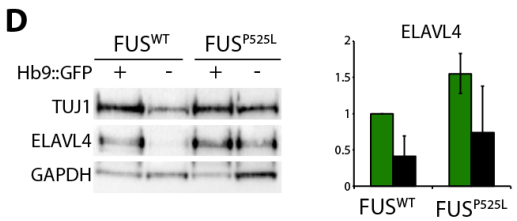
D
FUSWT
FUSP525L
Hb9::GFP
+
-
+
-
TUJ1
ELAVL4
GAPDH
ELAVL4
2
1.5
1
0.5
0
FUSWT
FUSP525L

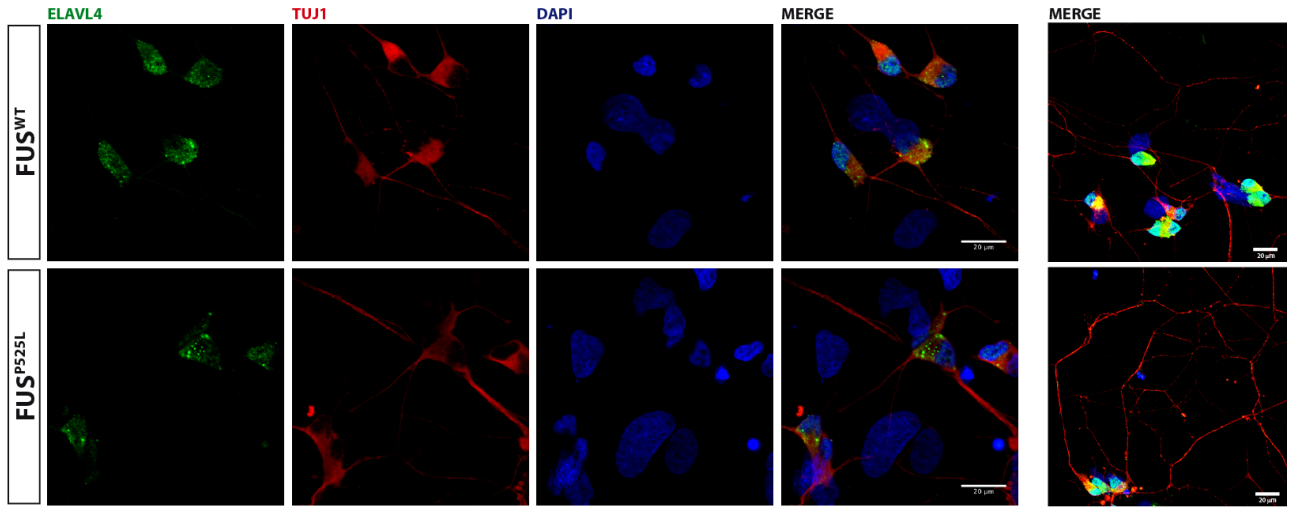
E
ELAVL4
TUJ1
DAPI
MERGE
MERGE
FUSWT
FUSP525L

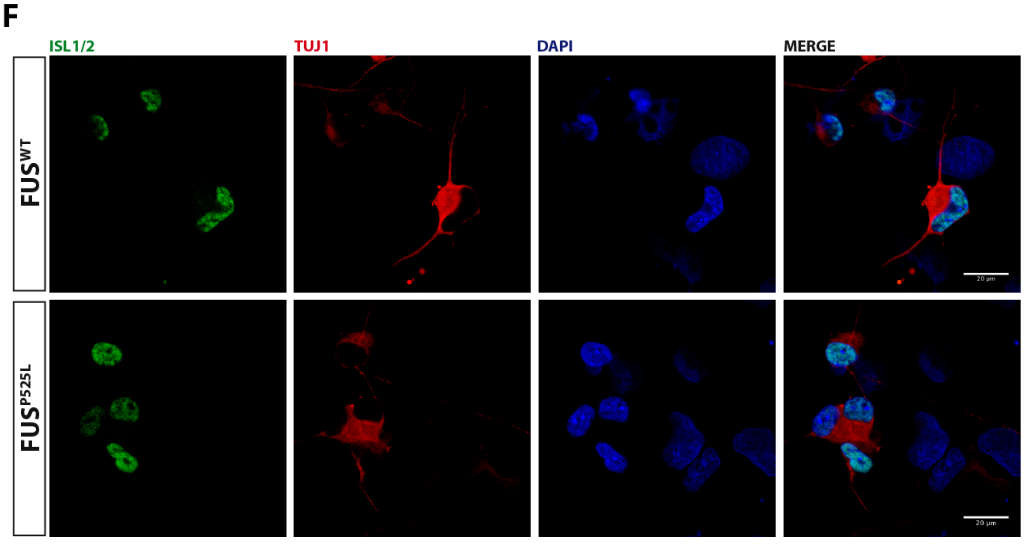
F
ISL1/2
TUJ1
DAPI
MERGE
FUSWT
FUSP525L

Figure S5. *ELAVL4* is a neural gene enriched in the Hb9::GFP-positive motor neuron population, Related to Figure 4

(A) Violin plot representing *ELAVL4* expression levels in different human tissues from the GTEx Portal (https://www.gtexportal.org/home/). Expression values are shown in TPM (Transcripts Per Million), calculated from a gene model with isoforms collapsed to a single gene. (B) Reads per kilobase per million mapped reads (RPKM) values for the indicated genes from our previous RNA-seq analysis of sorted Hb9::GFP-positive (green bars) and -negative (black bars) cells at day 12 of differentiation (De Santis et al., 2017) (*= false discovery rate < 0.05; ***= false discovery rate < 0.001). (C) RNA levels of the indicated genes by real time qRT-PCR in sorted Hb9::GFP-positive (green bars) and -negative (black bars) cells at day 12 of differentiation. Histogram bars represent the average of 4 independent experiments and error bars indicate the standard deviation (Student's t-test; paired; two tails; *= $p<0.05$). (D) TUJ1 and ELAVL4 protein quantification by western blot in sorted Hb9::GFP-positive and -negative cells at day 12 of differentiation. Right: densitometric analysis of ELAVL4 bands, normalized for GAPDH. Histogram bars represent the average of 3 independent experiments and error bars indicate the standard deviation. (E) Immunostaining for ELAVL4 (green) and TUJ1 (red) in FUS^{WT} and FUS^{P525L} mixed populations at 12+4 days of differentiation. DAPI (blue) stains nuclei. Scale bar: 20 μm. (F) Immunostaining for ISL1/2 (green) and TUJ1 (red) in FUS^{WT} and FUS^{P525L} mixed populations at 12+4 days of differentiation. DAPI (blue) stains nuclei. Scale bar: 20 μm.

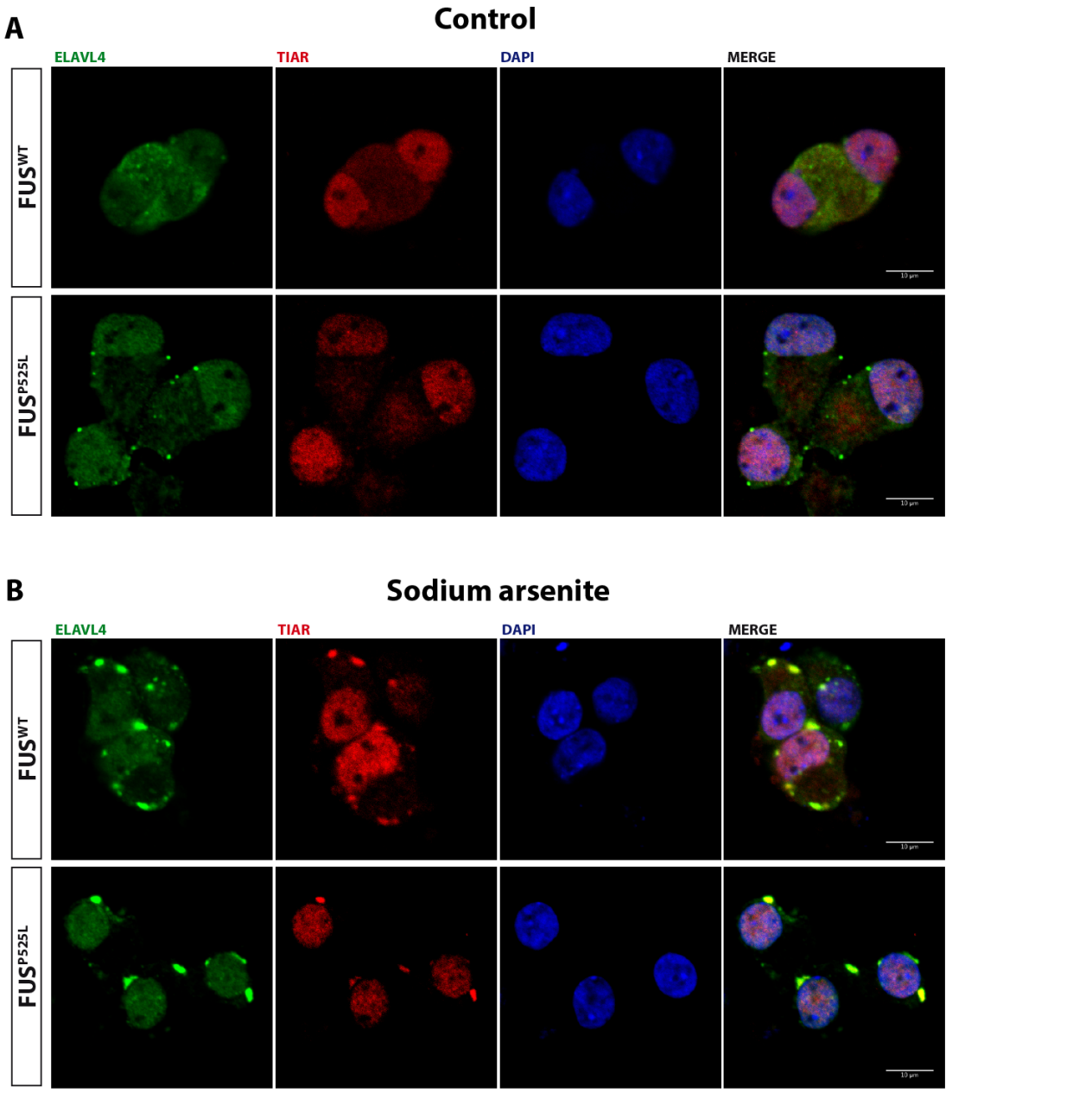
A
Control
ELAVL4
TIAR
DAPI
MERGE
FUSWT
FUSP525L
B
Sodium arsenite
ELAVL4
TIAR
DAPI
MERGE
FUSWT
FUSP525L
C
Control
ELAVL4 speckles volume
p=0.13
µm3
FUSWT#2
FUSP525L#2
ELAVL4 speckles mean intensity
p<0.0001
Arbitrary units
FUSWT#2
FUSP525L#2
D
Sodium arsenite
ELAVL4 SGs volume
p=0.73
µm3
FUSWT#2
FUSP525L#2
ELAVL4 SGs mean intensity
p=0.016
Arbitrary units
FUSWT#2
FUSP525L#2

Figure S6. ELAVL4 localization in SGs and speckles, Related to Figure 4

(A) and (B): single channels of the immunostaining reported in Figure 5A' and 5B', respectively, showing localization of ELAVL4 (green) and of the SG marker TIAR (red). DAPI (blue) stains nuclei. (C) and (D): quantitative analyses, as in Figure 5, of ELAVL4 speckles and SGs in FUS^{WT}#2 (n=16 for Control; n=20 for Sodium Arsenite) and FUS^{P525L}#2 (n=14 for Control; n=17 for Sodium Arsenite) MNs, derived from an independent pair of isogenic FUS wild-type and mutant iPSCs (De Santis et al., 2017). In all graphs the bars indicate the median with interquartile range. *p* values from Student's t-test (unpaired; two tails) are indicated.

A

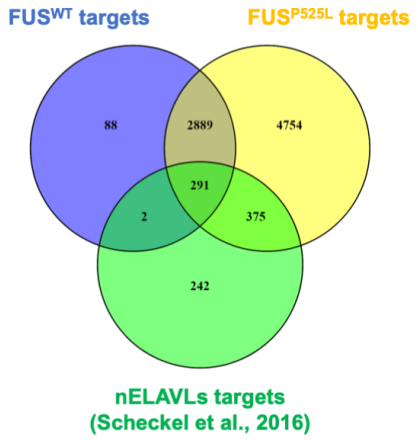

B

ELAVL4 top 30 targets (Tebaldi et al., 2018)	FUS^{WT} 5'UTR	FUS^{WT} CDS	FUS^{WT} 3'UTR	FUS^{P525L} 5'UTR	FUS^{P525L} CDS	FUS^{P525L} 3'UTR
CD9						✓
ACSL4					✓	✓
HMGB1						✓
LSM5					✓	✓
VDAC1					✓	✓
UBQLN2					✓	✓
TCF4						✓
SEMA4D						✓
CCT2		✓		✓	✓	✓
PDPK1						✓
PABPC1	✓	✓		✓	✓	✓
EEF1A1	✓	✓		✓	✓	✓
YWHAZ	✓		✓	✓		✓
STX12			✓		✓	✓
ACTG1			✓	✓	✓	✓
PPP2CA			✓	✓	✓	✓
MATR3	✓	✓	✓	✓	✓	✓
EIF2S3			✓		✓	✓
RAB11A	✓	✓	✓	✓	✓	✓
CD47		✓	✓	✓	✓	✓
TMEM30A			✓	✓	✓	✓
CDC42			✓		✓	✓
CALR	✓	✓	✓	✓	✓	✓
B2M		✓	✓	✓	✓	✓
RHOA			✓		✓	✓
RAC1			✓	✓	✓	✓
EIF4A1	✓	✓	✓		✓	✓
YBX1			✓		✓	✓
RPL27		✓	✓	✓	✓	✓
PFN1		✓	✓		✓	✓

Figure S7. ELAVL4 and FUS shared targets, Related to Figure 4

(A) Venn diagram showing the overlap between genes identified as targets of FUS^{WT} and FUS^{P525L} in the present work and ELAVL2, ELAVL3 and ELAVL4 (collectively, nELAVLs) by Scheckel et al. (2016). In the Scheckel et al. dataset, which derives from CLIP-seq in human brain samples, 95.5% of the reads were mapped in introns and 3'UTRs. Since we were looking for those candidates that might mediate the interaction of ELAVL4 and FUS in the cytoplasm, we have included in this analysis the 3'UTR nELAVLs targets and mRNAs bound in the exons by FUS^{WT} and FUS^{P525L}. (B) Table showing the top 30 ELAVL4 mRNA targets identified by Tebaldi et al. (2018) in NSC-34 cells. Overlap with the PAR-CLIP of the present work (exon bound mRNAs only) is indicated.

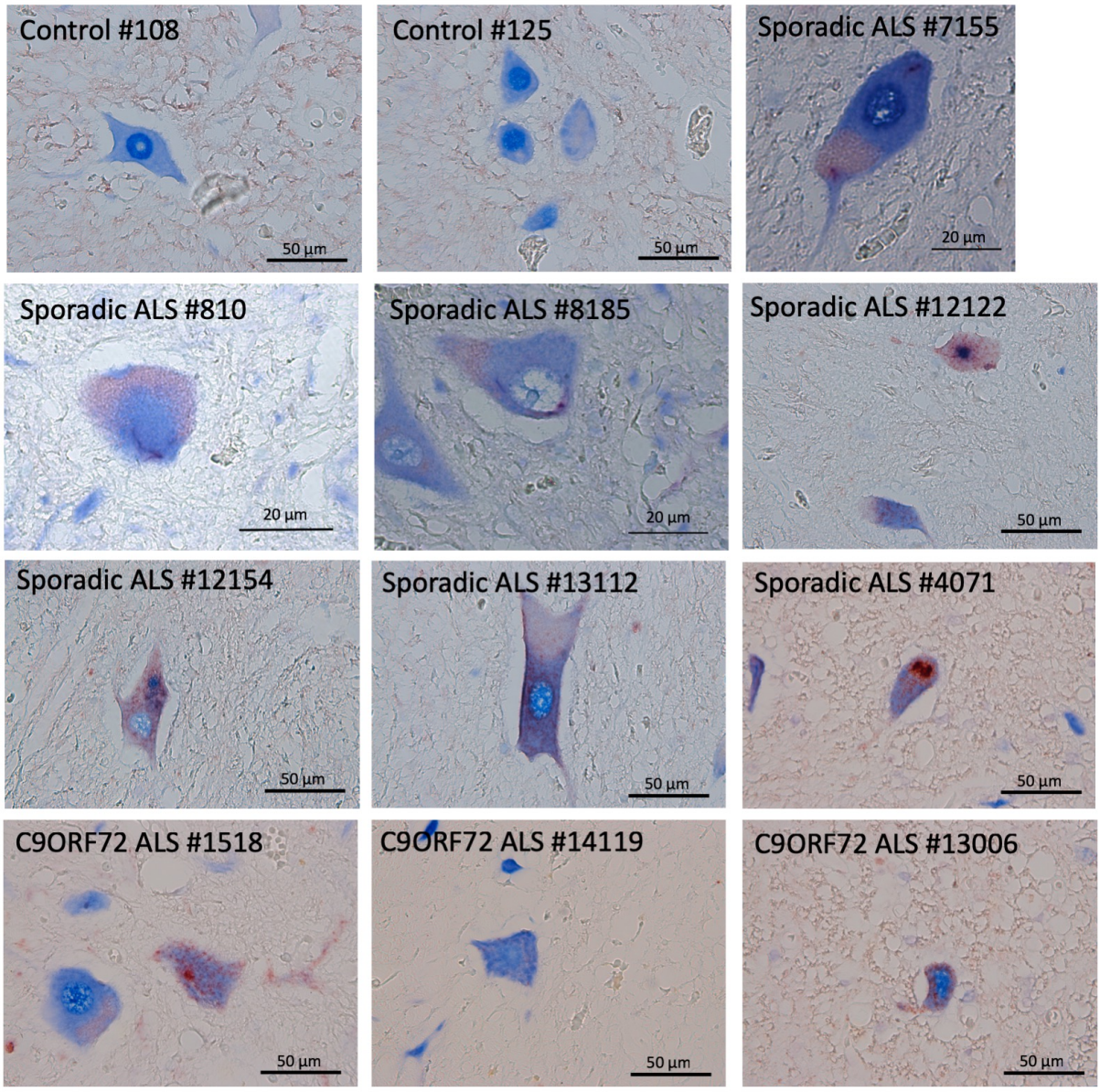

Figure S8. ELAVL4 localization in sporadic and C9ORF72 ALS patients' specimen, Related to Figure 6

Immunohistochemistry on spinal cord samples from controls, sporadic ALS patients and C9ORF72 pateints. For double immunohistochemistry, sections were labeled with anti-ELAVL4 (blue) and anti-pTDP-43 (pS409/410) (red). Characteristics of patients and controls are reported in Table S3.

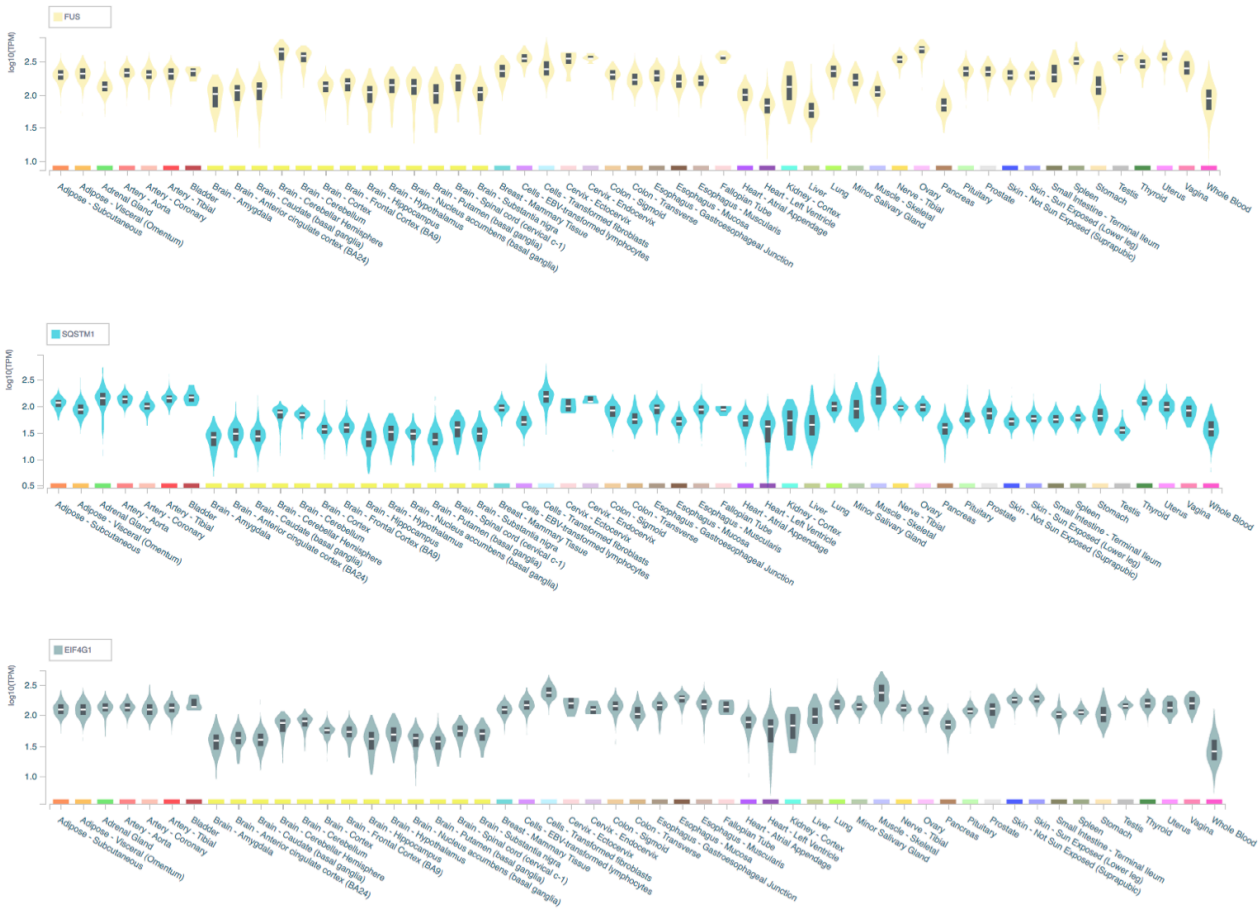

Figure S9. Ubiquitous expression of most components of the FUS-positive inclusions, Related to Figure 7

Violin plot representing expression levels of FUS (top), SQSTM1 (p62; middle) and EIF4G1 (bottom) in different human tissues from the GTEx Portal (https://www.gtexportal.org/home/). Expression values are shown in TPM (Transcripts Per Million), calculated from a gene model with isoforms collapsed to a single gene.

Table S2. Characteristics of FUS patients and controls used for immunohistochemistry of spinal cord sections, Related to Figure 5

	Age at death	Gender	Site & pattern of onset	Disease duration (months)
FUS^{R521C} (1)	41	M	bulbar	30
FUS^{R521C} (2)	70	F	limb	24
FUS^{R521H}	42	M	limb	88

	Age at death	Gender	Cause of death
Control	44	F	Sepsis – Mast cell Leukemia

Table S3. Characteristics of controls and sporadic and C9ORF72 familial patients used for immunohistochemistry of spinal cord sections, Related to Figure 6

Patient ID	Clinical diagnosis	Family history	Age of onset	Disease duration after diagnosis (months)	Gender	A: Thal phase amyloid	B: Braak stage tangles	C: plaque score
106	control	-	75	-	Male	A1	B0	C0
108	control	-	66	-	Female	A0	B1	C0
125	control	-	77	-	Female	A1	B1	C1
7155	ALS	N/A	53	30	Female	A0	B1	C0
810	ALS	N/A	63	32	Male	A0	B0	C0
8185	ALS	N/A	73	23	Male	A0	B1	C0
4071	ALS	N/A	54	20	Male	A0	B1	C0
12122	ALS	N/A	77	21	Male	A2	B2	C1
12154	ALS	N/A	70	25	Female	A0	B1	C0
13112	ALS	N/A	77	87	Male	A1	B0	C0
1518	C9ALS	N/A	78	14	Male	A0	B1	C0
14119	C9ALS	yes	69	45	Male	A0	B1	C0
13006	C9ALS	yes	64	57	Female	A0	B1	C0